Synthesis and Characterization of Cu-Al Alloy Nanoparticles Using Chemical Precipitation Method

J. Subhashini[1], A. Christy Ferdinand[*,2], T. Kasthuri[2]

[1]Research Scholar, PG & Research Department of Physics, Periyar Government Arts College, Cuddalore - 607001, Tamil Nadu, India.

[*,2]PG & Research Department of Physics, Periyar Government Arts College, Cuddalore - 607001, Tamil Nadu, India.

Abstract

In this work, nano structured Cu Al Alloy particles were synthesized by a chemical-precipitation method. The photo catalytic activities of the synthesized powders were investigated. The characteristics of synthesized powders were studied using a variety of techniques including X-ray diffraction, applied potential variation using Cyclic Voltammetry, Scanning Electron Microscopy with EDAX, Fourier transform infrared spectroscopy and ultraviolet-visible spectroscopy and Particle size Analyzer . The SEM results showed that CuAl nanoparticless are displayed agglomerated symmetrical and that the morphology of Cu Al alloy NPs of the single nanoparticles is flake like the flakes are 7.1 nm to 5.7 nm in dimensions for 300°c and 700°c. The similar shape of the CVs recorded at different scan rates indicates excellent electro chemical reversibility of the synthesized CuAl alloy nanoparticles.

Keywords: Cu, Al, SEM, EDAX, CV,UV, FTIR, XRD, PSA

Corresponding Author: christyferdinand2@gmail.com (A. Christy Ferdinand)

1. Introduction

Recently oxide spinels have gained a lot of attention because of their applications in the field of magnetic materials, pigments, catalysts, optical materials, etc. [1–3]. Among the many types of oxide spinel materials, CuAl show a high catalytic property. In addition, copper aluminate has a high thermal stability, high mechanical resistance, hydrophobicity and low surface acidity [4]. Conventional method to synthesize CuAl is solid-state reaction between Al and CuO which requires high temperature (above 1000 °C) and long period of calcination. These can cause grain growth in final product. In the recent years, wet chemical technologies have been employed to synthesize copper aluminate with high homogeneity, low calcination temperature and fine particle size. These methods involve sol–gel [5–7], sonochemical [4,8], reverse microemulsion [9], and other related methods. Among these methods, chemical-precipitation process is one of the interesting methods because of the inexpensive raw materials, a simple synthesis procedure and commonly available apparatus [10,11].

We seek to identify the impacts of the crystallinity, morphological variations, structural modifications, and electronic structure of nanomaterials like CuAl NPs addressing various challenges and offering solutions across diverse fields. In this context, our study aims to systematically investigate the effects of annealing temperature on the structural, optical, and morphological properties of synthesized nanomaterials through the chemical precipitation method. Employing a multidimensional characterization approach encompassing XRD, EDAX, FTIR, UV-Vis spectroscopy, SEM, CV, and PSA, our research endeavors to provide insights into the structural evolution, phase transformations, chemical bonding, optical behavior, surface morphology, and particle size distribution of the nanomaterial at different annealing temperatures.

2. Experimental procedure

CuAl nanopowder was prepared by a chemical precipitation method using Cu(NO3)2 3H2O (Merck), Al(NO3)3 9H2O (Merck) and NaoH (Merck) as a precipitating agent. First, Cu(NO3)2 3H2O and Al(NO3)3 9H2O in their respective stoichiometry (20 mmol aluminum nitrate and 10 mmol copper nitrate) were dissolved in 15 mL de-ionized water. After continuous stirring for 15 min, a transparent solution was obtained. Then, diethylamine was added slowly to the solution until a precipitate formed. The resultant synthesis precipitate was washed with deionized water and dried at 80 °C for 24 h. The dried precipitate was calcined for 2 h in a furnace at different temperatures.

3. Characterization techniques

X-ray diffraction (XRD) patterns were acquired for the prepared samples using the powder XRD technique with Cu-Kα radiation (λ=1.54060 Å) at 40 KV and 30 mA. Fourier Transform Infrared (FTIR) spectra spanning the region of 4000-400 cm^{-1} were obtained with a Magna IR spectrometer 550 Nicolet. UV-visible spectra were recorded using the Jasco Nicolet 670 W Japan spectrophotometer. The super capacitor properties of the synthesized Cu Al alloy nanoparticles were determined using cyclic voltammetry (Eco Chemie Autolab PGSTAT12 Potentiostat). Additionally, Scanning Electron Microscopy (SEM) was employed to further investigate the detailed structure and morphology of the prepared samples. The Particle Size Analyzer (Nano Plus Micromeritics) was utilized for analyzing the particle size distribution.

4. Result and discussion

4.1 UV STUDIES

Figure1 shows the UV-VIS spectrum of synthesised Cu Al Alloy nanoparticles by chemical co-precipitation method at different temperatures, it reflects the variation of % absorbance of Cu Al Alloy function of wavelength from 200 to 800 nm. It was evident from spectra [12] that the absorption peak of metal nanoparticles mostly lies in the UV region of spectrum [14,15]. Though Cu nanoparticle typically shows its absorption in the visible region [13,14] but the absorption peak of such nanoparticles lies in the UV range owing to their oxidation behaviour. It was also observed that the absorption intensity of alloy nanoparticle is significantly higher than Cu and Al nanoparticles. In previous studies, Cu NPs showed SPR in an area around 562–573 nm [16-18].

The broad band is observed of Aluminium Oxide towards blue shift at 345.4 nm [19,20]. A smaller absorption edge is advantageous for simpler electronic conductivity (greater energy transformations) and consequently quicker ionic conductivity. However, in our work, SPR was observed in the area around 255.5 nm and 421.5 nm for different annealed temperatures 300°c and 700°c. On comparisons of the present study with literature reveals that Cu Mg Alloy nanoparticles has led to a shift in the fundamental optical absorption edge towards the Ultra Violet (UV) region. It was probably due to the position of Plasmon absorption peak which depends on several factors: the particle size, shape, type of solvent, The absorption data obtained were extrapolated to the Tauc relation the plot of $(\alpha h\nu)^2$ versus the energy of the photons ($h\nu$), where α is the absorbance value, h is the Plank constant, and ν is the frequency of the photons.

When the absorption data are traced by the Tauc relation, it will show one or more straight lines these lines will intercept with the energy (hv) axis, and this intercept gives the value of the energy gap (Eg) and it is shown in shown in figure 2.The bandgap energy of Cu Al Alloy nanoparticle was found to be 5.82 eV, 5.88 eV for 300°c and 700°c. Further, many authors [13-15] have calculated the bandgap of different metal nanoparticles from their absorption spectra. Bandgap around 5.2 eV, 4.8 eV and 4.5 eV were calculated for Cu-Al, Cu and Al nanoparticles respectively. It was evident from the absorption spectra that the band gap of alloy particle is larger than the pure particles which are similar to our studies.

The variation of extinction coefficient with wavelength is shown in Figure 3. The extinction coefficient (K) is a measure of the fraction of light lost due to scattering and absorption per unit distance of the penetration medium. The extinction coefficient is computed in the sample during the exposure of UV spectra by using the relation between % absorption and wavelength [21]. Extinction coefficient (K) is calculated from the formula

$$K = \frac{\alpha\lambda}{4\pi}$$

where α is % absorption and $\lambda$is wavelength. The curve of extinction coefficient clearly shows that scattering decreases gradually from 400 nm up to 1100 nm for constant distance of the penetration medium.

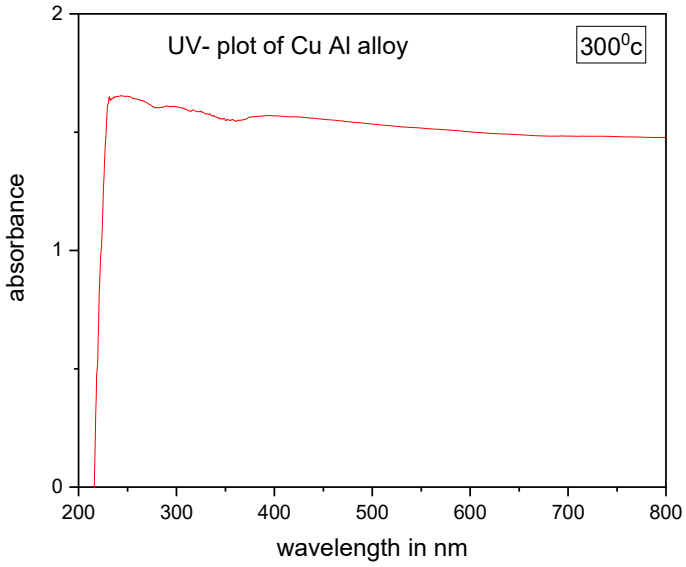

Figure 1a uv plot of cu al alloy at 300°c

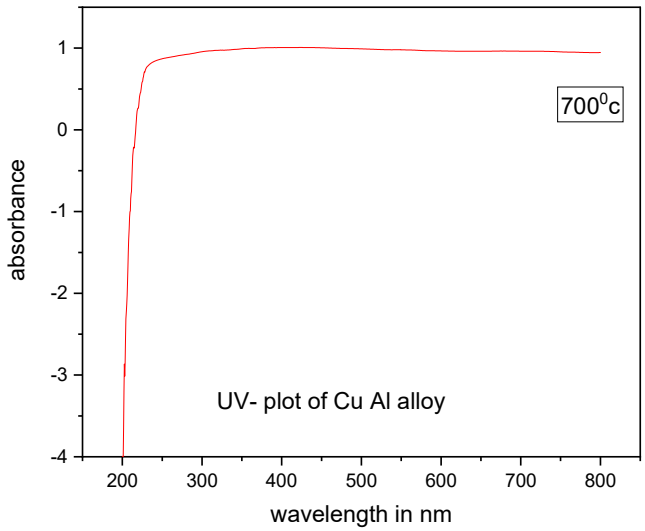

Figure 1b uv plot of cu al alloy at 700°c

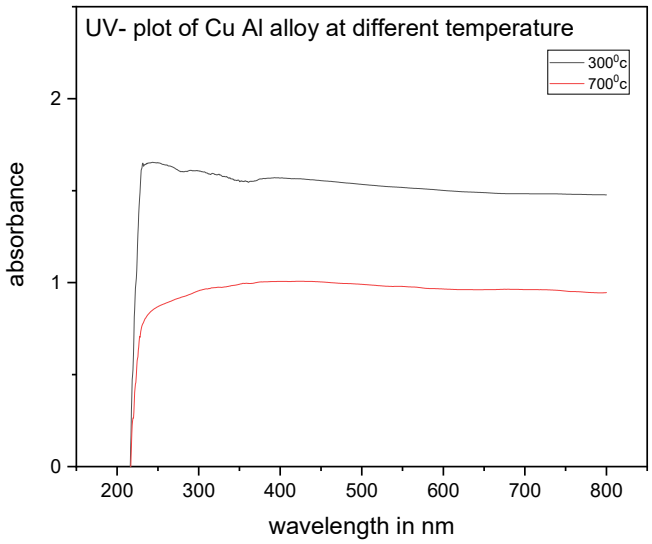

Figure 1c uv plot of cu al alloy at different annealed temperature

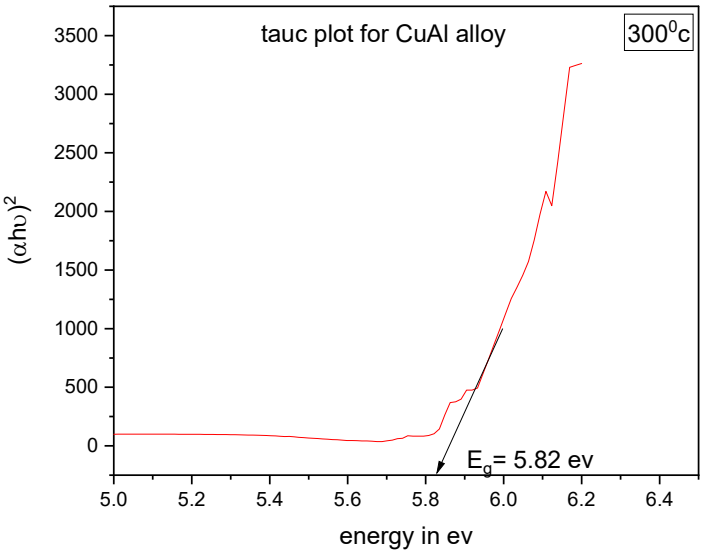

Figure 2 a tauc plot of cu al alloy at 300°c

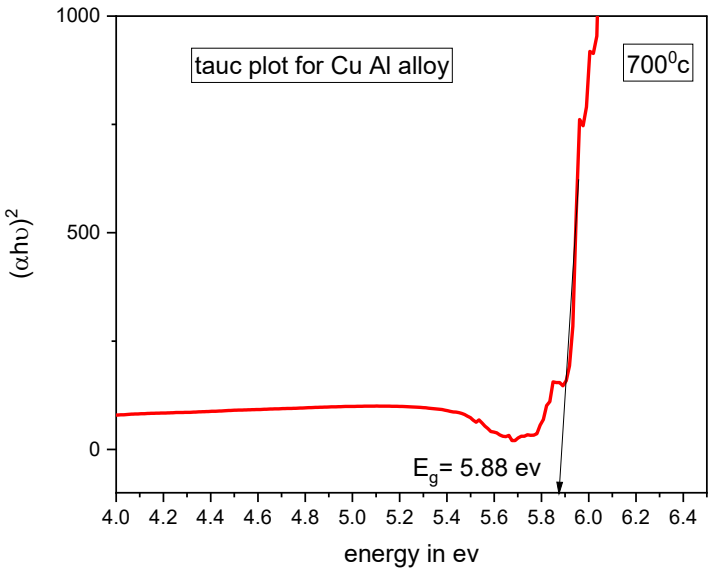

Figure 2b tauc plot of cu al alloy at 700°c

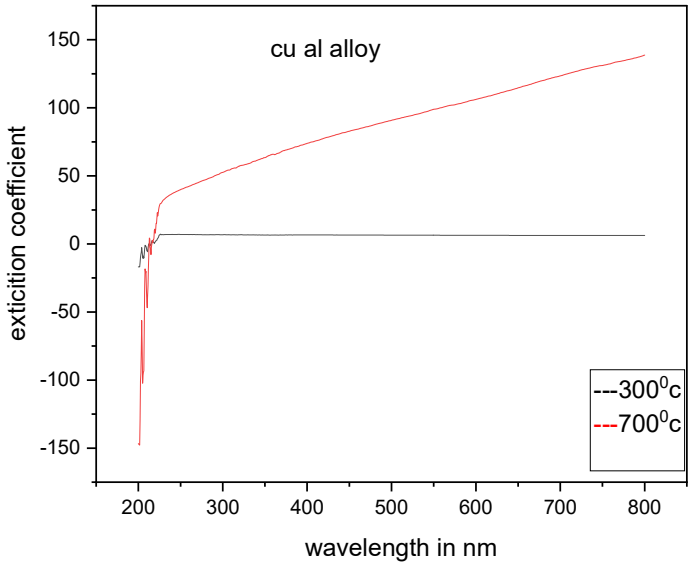

Figure 3 k vs λ plot of cu al alloy at different annealed temperatures

4.2 SEM STUDIES

We can see from the SEM images (Fig. 4)and zoom view that the nanostructure of Cu Al alloy particles displayed agglomerated symmetrical and that the morphology of Cu Al alloy NPs of the single nanoparticles is flake like the flakes are 7.1 nm to 5.7 nm in dimensions for 300°c and 700°c this is to some extent due to the interaction between the nanoparticles, Heat treatment resulted in agglomeration of the powder as a function of the calcining temperature which is typical for the alloy samples. Therefore, some degree of agglomeration at the higher calcination temperature appears unavoidable. In many cases of Nano crystalline materials, it is observed that there is a tendency of agglomeration among the nanoparticles [22]. These particles are fluxes, sphere and fracture in shape which is a typical result of precipitation method. Low resolution image of prepared copper aluminium alloy at different temperatures exhibits a clusters morphology. High resolution SEM images shows synthesised NPS are grown highly crystalline.

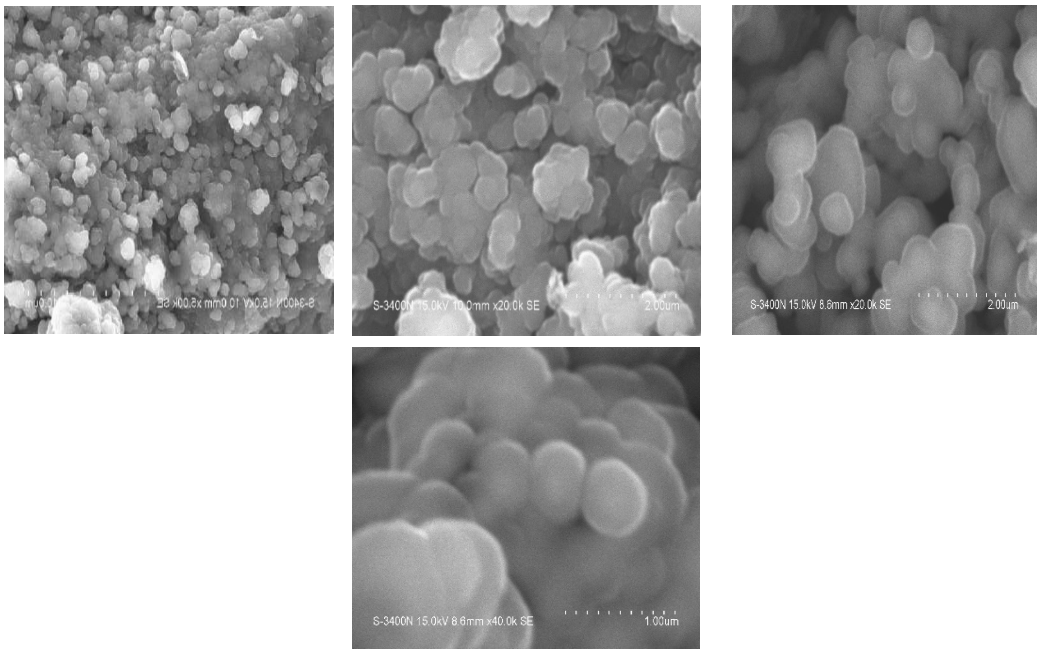

Figure 4 a depicts the SEM micrographs of sample Cu Al alloy nanoparticles for different magnification at 300 ^{0} C

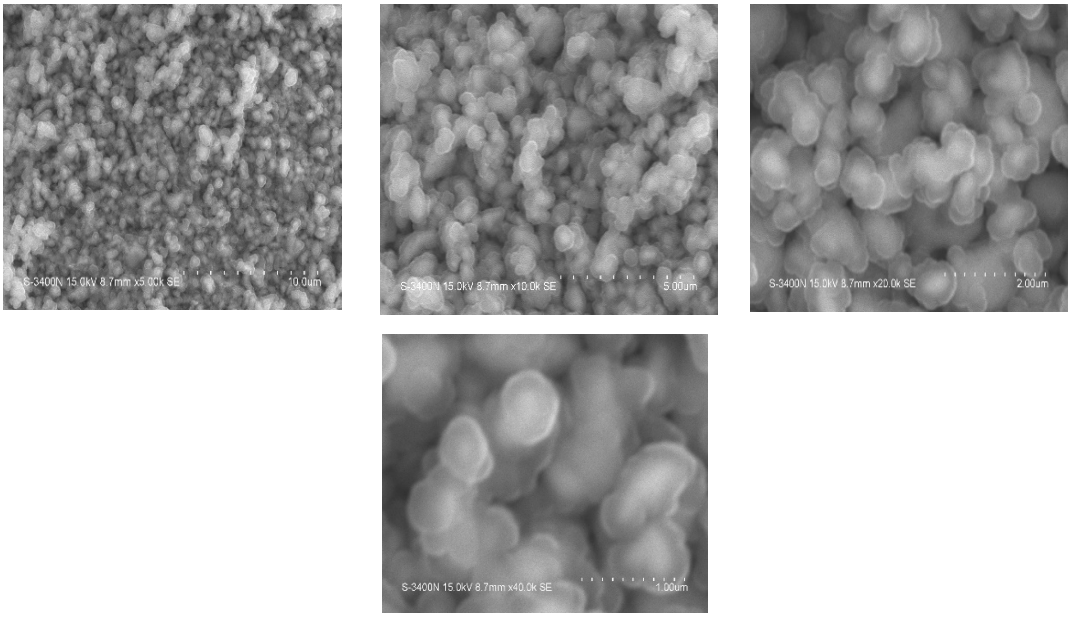

Figure 4b depicts the SEM micrographs of sample Cu Al alloynanoparticles for different magnification at 700 ^{0} C

4.3 EDAX STUDIES

Energy dispersive X-ray analysis (EDX) is performed in conjunction with SEM or TEM. It provides the elemental details of near surface elements of a sample and the overall positional mapping in it. Here a high energy electron beam ~ 10–20 keV is bombarded on a sample and X-rays emitted from the sample are collected by an energy dispersive spectrometer. The energy of the X-rays generated are characteristics of the atomic structure of the element from which it is emitted, and hence provides the elemental details of the sample. X-rays are generated in approximately 2 μm depth of the sample and, therefore,

EDX is generally a bulk characterization technique. The electron beam is scanned across the sample to verify the spatial uniformity and homogeneity.

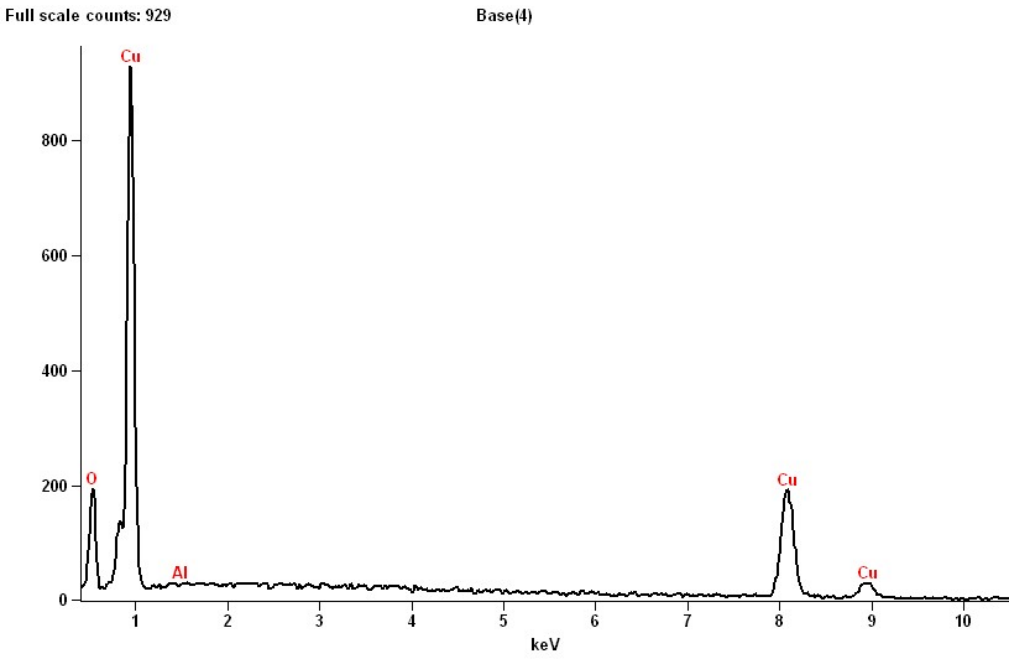

Table 1

Element Line	*Net Counts*	*Net Counts Error*	*Weight %*	*Atom %*	*Formula*
O K	846	+/- 71	9.46	29.33	O
Al K	3	+/- 26	0.01	0.03	Al
Cu K	3513	+/- 123	90.52	70.64	Cu
Cu L	8526	+/- 121	---	---	
Total			100.00	100.00	

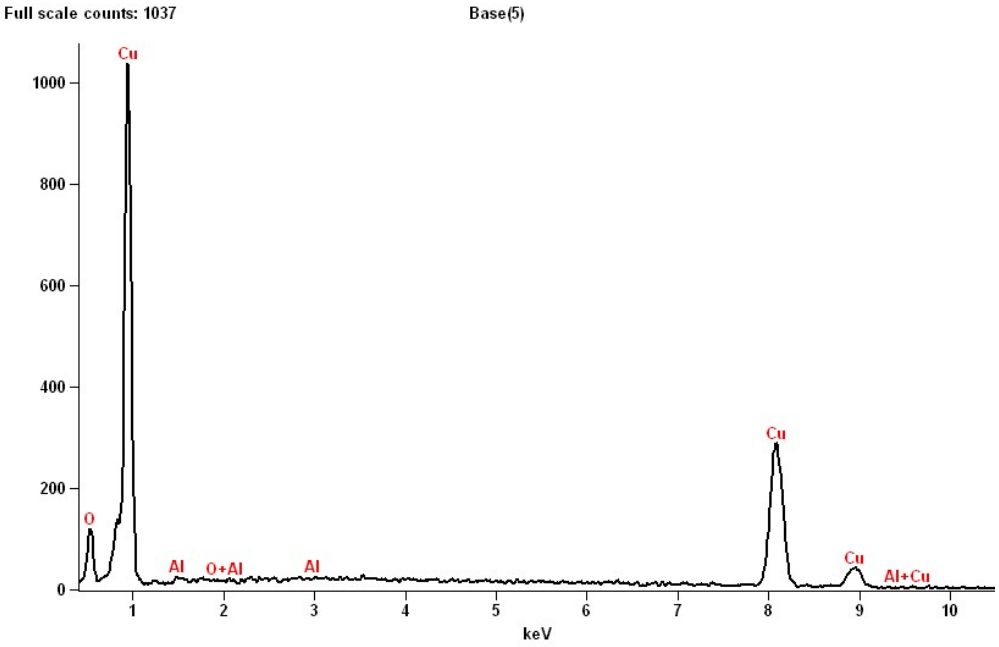

Table 2

Element Line	Net Counts	Net Counts Error	Weight %	Atom %	Formula
O K	605	+/- 57	4.77	16.53	O
Al K	103	+/- 21	0.39	0.81	Al
Cu K	5388	+/- 145	94.83	82.66	Cu
Cu L	9293	+/- 121	---	---	
Total			100.00	100.00	

EDAX analysis gives qualitative as well as quantitative status of elements that may be involved in formation of nanoparticles. Figure 1 shows elemental profile of synthesized nanoparticle copper aluminum alloy. TABLE 1 and 2gives the true elemental composition of the nanoparticles. The analysis revealed highest proportion of Copper (90.52%) in nanoparticle followed by oxygen (9.46%), and aluminum(0.01%).

4.4 FTIR STUDIES

The light transmittance properties of the copper aluminum alloy NPs were studied via FTIR as shown in figure1. FTIR, like UV-Vis, enables compounds to be identified given that each compound exhibits distinct transmittance bands when exposed to IR light. The FTIR spectra of the sample copper aluminum alloy prepared by chemical co precipitation method are presented in Figure. Figure 1a and 1b shows the FTIR spectra of the sample annealed at two different temperatures namely 300°c and 700°c. It is evident from the figure that, the samples give rise to absorption bands in the range of 4000 to 400 cm^{-1}.

The broad band centered at 3462 cm^{-1} can be attributed to the stretching vibrations of O-H functional group. The medium intensity sharp band at 1640 cm^{-1} can be associated with the bending vibrations of O-H functional group. The existence of these two bands confirms the presence of water molecules adsorbed from the environment on the surface of the nanomaterial due to their high specific surface areas [23,24]. The sharp and medium intensity bands at 2926.1 cm^{-1} can be assigned to C-H stretching bonds. These bands invariably appear in the FTIR spectra of samples and they are seldom considered important in determining the structure [23]. The transmittance band at 1646 cm^{-1} is attributed to the C-C stretching mode. Furthermore, the large transmittance band at 1384cm^{-1} is ascribed to the C-H bending mode.

The sharp peak at 1122 cm^{-1} corresponds to C-O stretching of strong intensity of aliphatic ether or tertiary alcohols but the absorption peaks from 814 to 571.23 cm^{-1} suggest strong bands in the finger printing region could also be attributed to oxygen-metal vibration which hints at the formation of metal oxides [25].

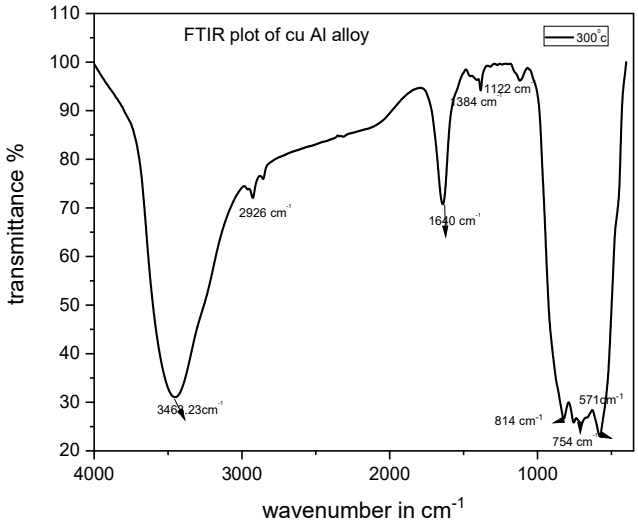

Figure 5a. FTIR Plot of Cu Al alloy at annealed temperature 300°C

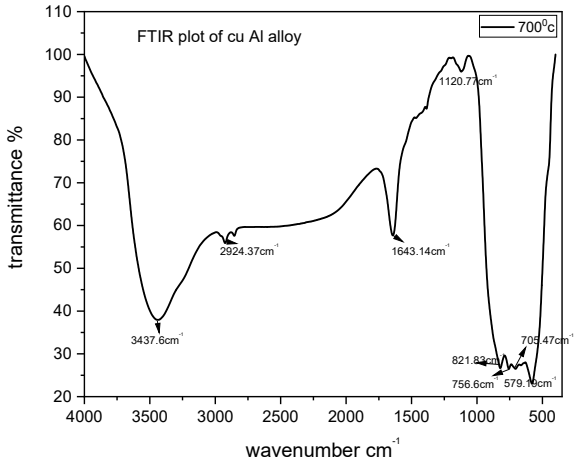

Figure 5b. FTIR Plot of Cu Al alloy at annealed temperature 700°C

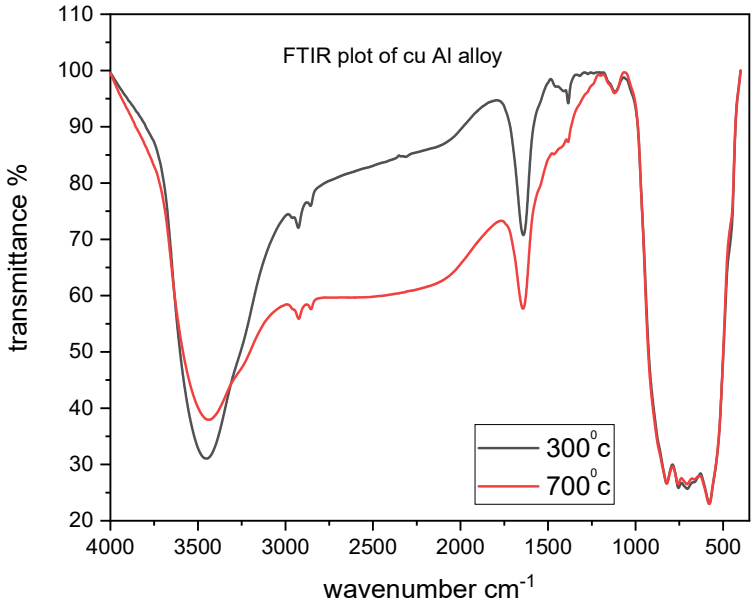

Figure 5c. FTIR Plot of Cu Al alloy at different annealed temperatures

4.5 PSA STUDIES

Copper aluminum alloy nanoparticles samples annealed at two different temperatures 300°c and 700°c were analyzed using particle analyzer to estimate the particle size. Cu Al alloy nanoparticles were suspended in water and kept in ultra-sonication for 5 min. Figure 6 shows the result of the analyzed sample. The average size of the particle was calculated to be 919.3 d nm and 605.3 d nm for the synthesized Cu Al alloy nanoparticles at 100% intensity at different annealed temperatures.

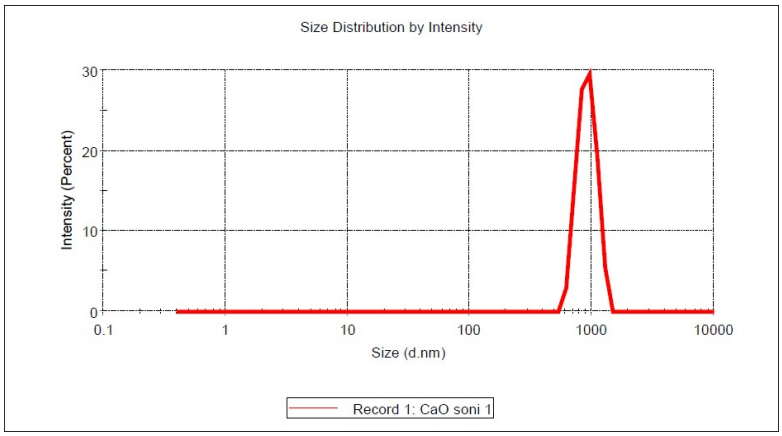

Figure 6a PSA Results of Cu Al alloy nanoparticles 300°C

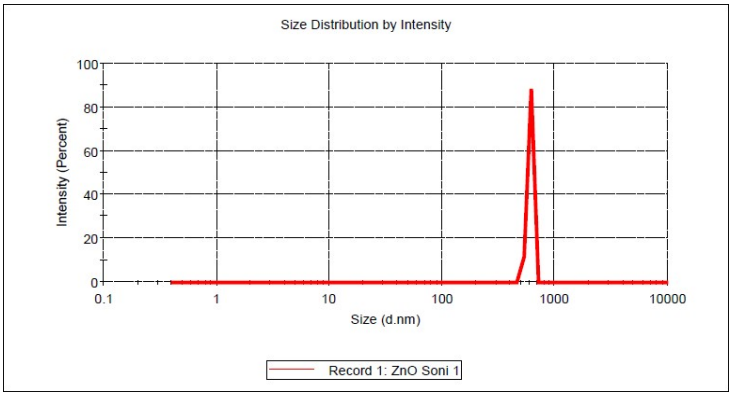

Figure 6b PSA Results of Cu Al alloy nanoparticles at 700°C

4.6 XRD STUDIES

XRD spectra of copper aluminium alloy-NPs obtained from chemical co precipitation synthesis at different annealed temperatures are shown in Figure 7. It clearly exhibits the peaks at angles 5.6662°, 32.7952°, 37.4134°, 45.5011°, 57.6847°, 60.8563° and 67.4496°. Which reveals the information that sharp and intense peaks indicate the synthesized nanoparticles are crystalline in nature. The XRD peak profile analysis is done for as-prepared and annealed copper aluminium alloy sample.

Basically the X-ray line broadening is mainly due to three factors namely instrumental effect, crystalline size and local lattice strain. In order to exclude the instrumental broadening, a standard silicon X-ray powder diffraction data is recorded under the same condition and is eliminated from the observed peak width. But the latter two contributions cannot separate directly and hence Williamson-Hall (W-H) plots are used. The full width at half maximum (FWHM) of all the sample is estimated using a nonlinear curve fitting function called Gaussian, which gives the best fit for the experimental data. As the width of the peak increases size of particle size decreases, which resembles that present material in an orange [26,27].

The average crystallite size (D) of the sample is calculated using Debye-Scherer's formula which can be given

$$D = \frac{K\lambda}{\beta COS\theta}$$

Where K is the shape factor (0.90), λ is the wavelength of Cu K_α radiation (λ=1.5406Å), β is the full – width at half maximum, and θ is the diffraction angle. The average grain size of copper aluminum alloy – NPs is found to be~10nm and 16 nm at different annealed temperatures at 300°C, 700°C respectively.

Additionally the dislocation density(δ), which represents the amount of defects in the sample is defined as the length of dislocation lines per unit volume of the crystal and is calculated using Williamson and small man's formula [28] in $lines/m^2$

$$\delta = \frac{n}{D^2}$$

where n is approximately equal to 1 [27], D is the crystallite size. The dislocation density (d) is found to be1 $\times 10^{16}$lines $/m^2$ and 3.906×10^{15} $lines/m^2$ sample

copper aluminium alloy-NPs different annealed temperatures at 300°C, and 700°C respectively.

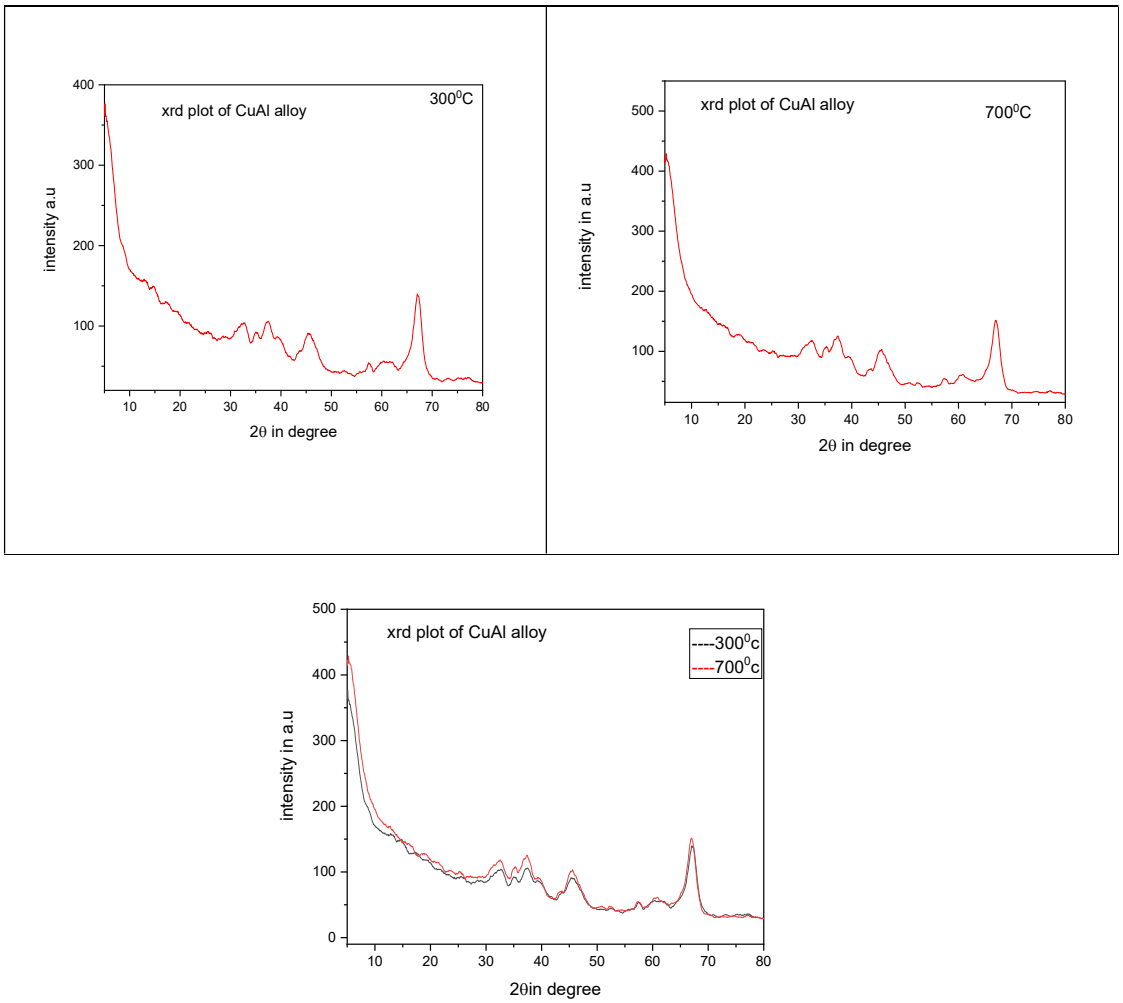

Figure 7 XRD plot of copper aluminiumalloy-NPsat different temperatures

Williamson–Hall Method of Analysis

The Scherrer equation focuses only on the effect of crystallite size in XRD peak broadening and it cannot be considered for microstructures of the lattice, i.e., about the intrinsic strain, which becomes developed in the Nano crystals through the point defects, grain boundaries, triple junctions, and stacking faults [29]. One of the methods considering the effect of strain-induced XRD peak broadening is the Williamson–Hall

(W-H) method; also, this method provides calculation of the crystal size along with the intrinsic strain [30,31]. According to the physical line broadening of X-ray diffraction peak, it is a combination of size and strain. The W-H method does not confirm a 1/cosθ dependency as in the Scherrer equation but varies with tanθ in strain considerations. This basic difference pursues a dissociation of broadening reflection and combines small crystallite size and microstrain together. The distinguished θ associations of both effects of size and strain broadening in the analysis of W-H are given as Equation

$$\beta_{total} = \beta_L + \beta_\epsilon$$

where

$$\beta_L = \frac{K\lambda}{L\cos\theta} \quad \text{and} \quad \beta_\varepsilon = 4C_\epsilon \tan\theta$$

If both contributions are present then their combined effect should be determined by convolution. The simplification of W-H method is to assume the convolution as a simple sum. Using the former of these then we get

$$\beta_{total} = \frac{K\lambda}{L\cos\theta} + 4C_\epsilon \tan\theta$$

If we multiply this equation by cosθ we get:

$$\beta_t \cos\theta = \frac{K\lambda}{L} + 4C_\epsilon \sin\theta$$

Comparing this with the standard equation for a straight line y =mx + c, we see that by plotting $\beta_t \cos\theta$ versus 4sinθwe obtain the straight line with the slope Cϵ and the intercept $\frac{K\lambda}{L}$ that determines size of the crystal. Such a plot is known as a W-H plot and shown in Figure 8a, and 8b.

Crystal sizes by W-H plot for copper aluminium alloy-NPs sample at different annealed temperatures are 7.02 E-11 m, and 8.30 E-11 m respectively.

The slope Cϵ gives the micro strain, this may be due to the lattice shrinkage and the values are 0.4457×10^{-3} and 0.6543×10^{-3}

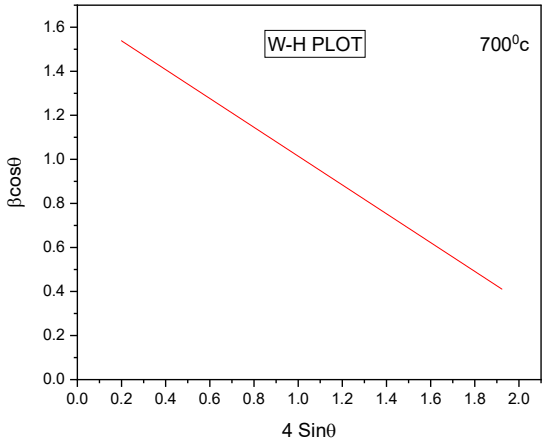

Figure 8a W-H plot for copper aluminium alloy annealed at 300°c

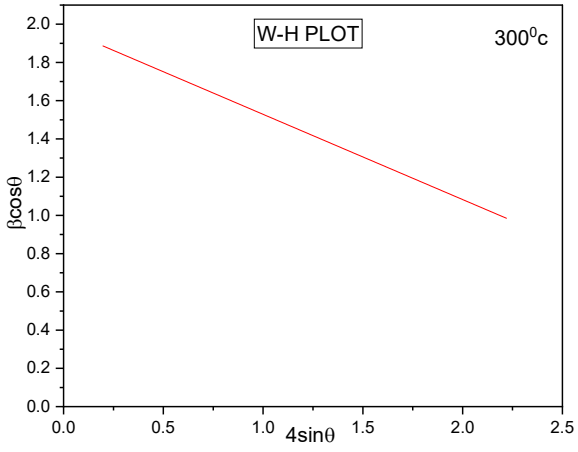

Figure 8b W-H plot for copper aluminium alloy annealed at 700°c

4.7 CYCLIC VOLTAMMETRY

The super capacitor properties of the synthesized Cu Al alloy nanoparticles were determined using cyclic voltammetry. The like voltammetry, were performed at room temperature. Figure 9(a), 9(b) shows measured cyclic voltamograms (CVs) recorded in the KOH electrolyte for the synthesized Cu Al alloy nanoparticles films at four different scan rates (50 to 100mVs^{-1}). CVs provid evaluable information on reduction oxidation (charge-discharge) behavior. Here, the capacitance was mainly based on the redox reaction because the shape of the CVs is distinguished from the shape of electric double-layer capacitance, which is normally close to an ideal rectangle [21].

As the scan rate was increased, the current response, which is a measure of the capacitance, increased. The similar shape of the CVs recorded at different scan rates indicates excellent electro chemical reversibility of the synthesized CuAl alloy nanoparticles.

The specific capacitance of the electrode can be calculated from the CV curves according to the following equation.

$$C = \frac{1}{ms(v_a - v_b)} \int Idv$$

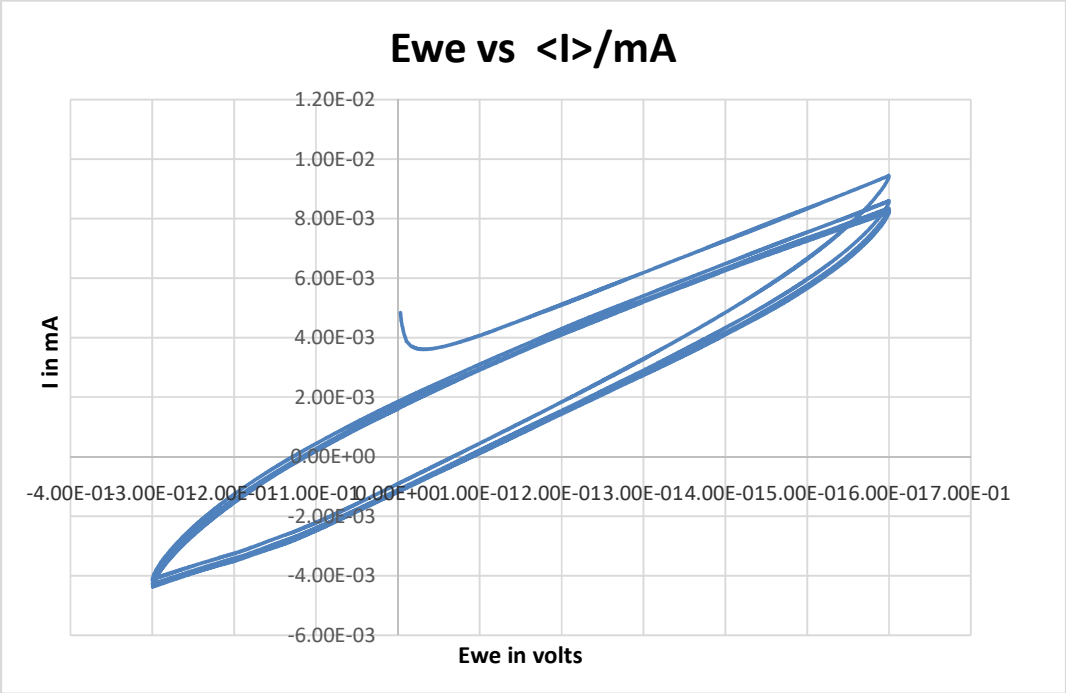

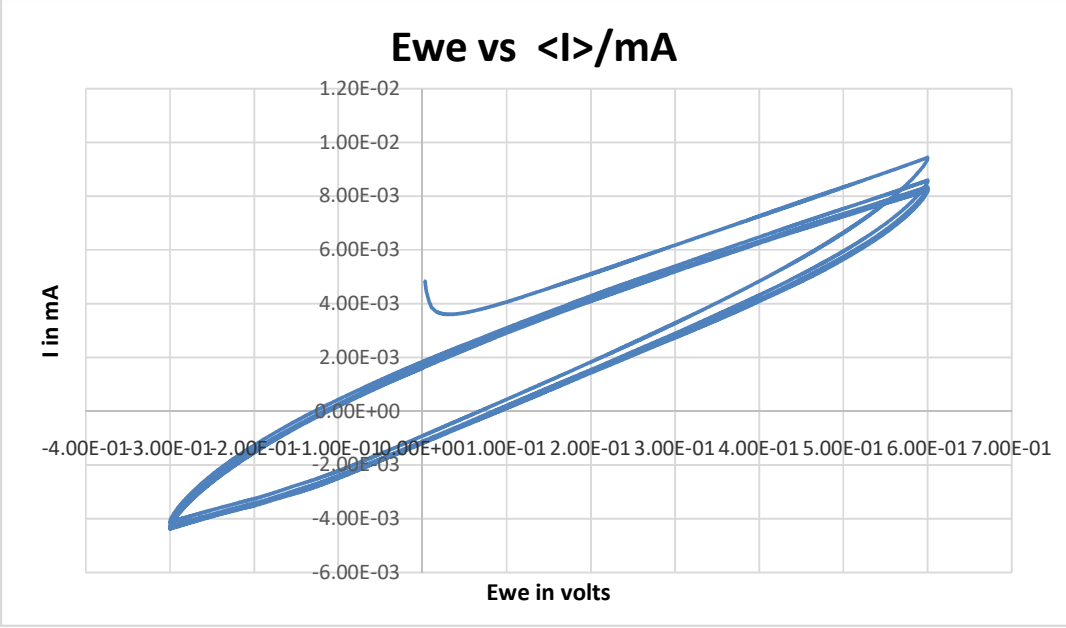

Figure 9a CV Curveof Cu Al alloy Nanoparticles at Different Scan Rate at 300°c

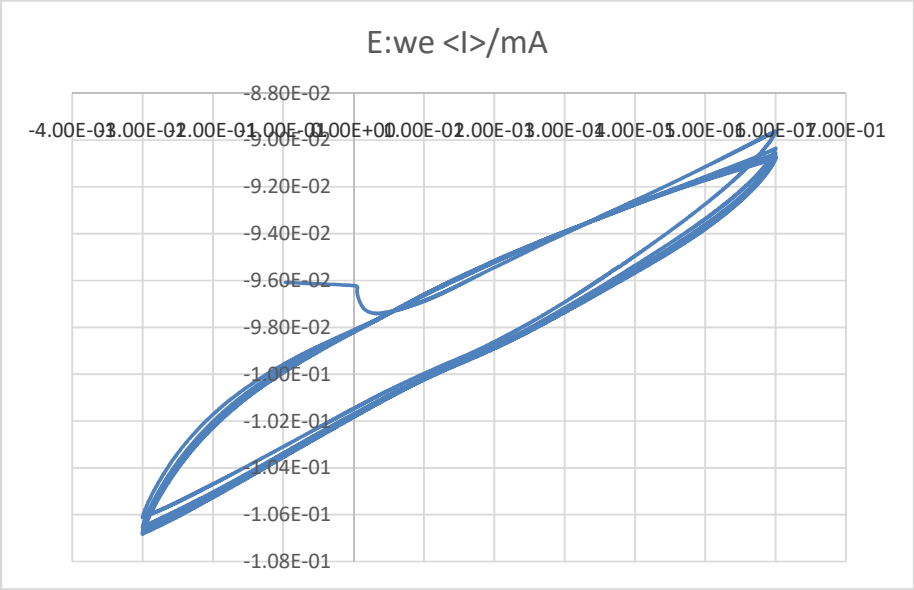

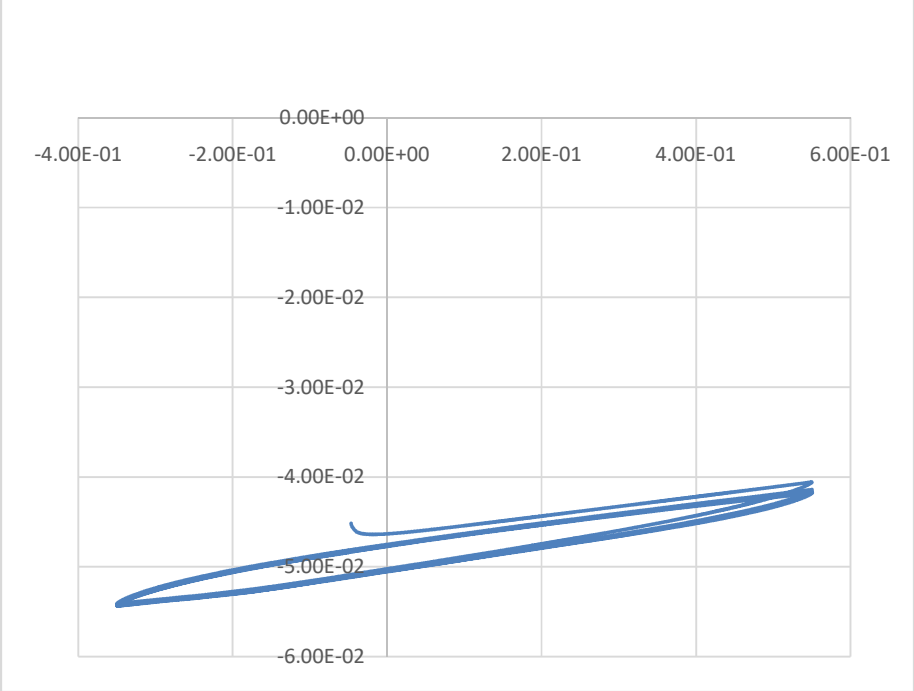

Figure 9b CV Curve of Cu Al alloy Nanoparticles at Different Scan Rate at 700°

5. Conclusion

Nanosized copper aluminate particles were synthesized using a co-precipitation method. These nanoparticles are flake like morphology and a particle size of about 605.3 d nm. The nanoparticles were characterized by several experimental techniques. The XRD reveals the information that sharp and intense peaks indicate the synthesized nanoparticles are crystalline in nature. Where Cyclic Voltometer provide evaluable information on reduction oxidation (charge-discharge) behavior. Additionally, these nanostructures exhibit promise in wastewater treatment for heavy metal and organic pollutant removal, as well as serving as eco-friendly flame retardants in polymer composites. Challenges in scalability, stability, and understanding mechanisms must be addressed for broader use, motivating future research in novel synthesis methods and application exploration.

REFERENCES

[1] M. Jafari, S.A. Hassanzadeh-Tabrizi, Preparation of CoAl2O4 nanoblue pigment via polyacrylamide gelmethod, Powder Technol. 266 (2014) 236–239.

[2] F. Foroughi, S.A. Hassanzadeh-Tabrizi, J. Amighian, Microemulsion synthesis and magnetic properties of hydroxyapatite- encapsulated nano CoFe2O4, J. Magn. Magn. Mater. 382 (2015) 182–187.

[3] S.A. Hassanzadeh-Tabrizi, Polymer-assisted synthesis and luminescence properties of MgAl2O4:Tb Nanopowder, Opt. Mater. 33 (2011) 1607–1609.

[4] W. Lv, B. Liu, Q. Qiu, F. Wang, Z. Luo, P. Zhang, S. Wei, Synthesis, characterization and photocatalytic properties of spinel CuAl2O4 nanoparticles by a sonochemical method, J. Alloy. Compd. 479 (2009) 480–483.

[5] B.K. Kwak, D.S. Park, Y.S. Yun, J. Yi, Preparation and characterization of nanocrystalline CuAl2O4 spinel catalysts by sol–gel method for the hydrogenolysis of glycerol, Catal. Commun. 24 (2012) 90–95.

[6] J. Yanyan, L. Jinggang, S. Xiaotao, N. Guiling, W. Chengyu, G. Xiumei, CuAl2O4 powder synthesis by sol-gel method and its photodegradation property under visible light irradiation, J. Sol–Gel Sci. Technol. 42 (2007) 41–45.

[7] M. Salavati-Niasari, F. Davar, M. Farhadi, Synthesis and characterization of spinel-type CuAl2O4 nanocrystalline by modified sol–gel method, J. Sol–Gel Sci. Technol. 51 (2009) 48–52.

[8] W. Lv, Z. Luo, H. Yang, B. Liu, W. Weng, J. Liu, Effect of processing conditions on sonochemical synthesis of nanosized copper aluminate powders, Ultrason. Sonochem. 17 (2010) 344–351.

[9] J. Chandradass, K.H. Kim, Synthesis and characterization of CuAl2O4 nanoparticles via a reverse microemulsion Method, J. Ceram. Process. Res. 11 (2010) 150–153.

[10] S.A. Hassanzadeh-Tabrizi, M. Mazaheri, M. Aminzare, S.K. Sadrnezhaad, Reverse precipitation synthesis and characterization of CeO2 nanopowder, J. Alloy. Compd. 491 (2010) 499–502.

[11] S.A. Hassanzadeh-Tabrizi, E. Taheri-Nassaj, Synthesis of high surface area Al2O3–CeO2 composite nanopowder via inverse co-precipitation method, Ceram. Int. 37 (2011) 1251–1257.

[12] Comparative study on Cu, Al and Cu-Al alloy nanoparticles synthesized through underwater laser ablation technique N Patra , R Patil , A Sharma , V Singh and I A

Palani1,IOP Conf. Series: Materials Science and Engineering 390 (2018) 012046 doi:10.1088/1757-899X/390/1/012046.

[13] Moniri S, Ghoranneviss M, Hantehzadeh M R and Asadabad M A 2017 Synthesis and optical characterization of copper nanoparticles prepared by laser ablation Bull. Mater. Sci. 40,1 pp 37–43.

[14] Sadrolhosseini A R, Noor A S B M, Shameli K, Mamdoohi G, Moksin M M and Adzir Mahdi M 2013 Laser ablation synthesis and optical properties of copper nanoparticles J. Mater. Res.28,18 pp 2629–2636.

[15] Mahdieh M H and Mozaffari H 2017 Characteristics of colloidal aluminum nanoparticles prepared by nanosecond pulsed laser ablation in deionized water in presence of parallel external electric field Phys. Lett. Sect. A Gen. At. Solid State Phys. 381,38 pp 3314–3323.

[16] Dang T.M.D., Le T.T.T., Fribourg-Blanc E., Dang M.C. Synthesis and optical properties of copper nanoparticles prepared by a chemical reduction method. *Adv. Nat. Sci. Nanosci. Nanotechnol.* 2011;2(1) [Google Scholar].

[17] Sampath M., Vijayan R., Tamilarasu E., Tamilselvan A., Sengottuvelan B. Green synthesis of novel jasmine bud-shaped copper nanoparticles. *J. Nano technol.* 2014; 2014:1–7. [Google Scholar].

[18] Suci Amaliyah,[a] Dwika Putri Pangesti,[a] Masruri Masruri,[a] Akhmad Sabarudin,[a,*] and Sutiman Bambang Sumitro[b] Green synthesis and characterization of copper nano particles using *Piper retrofractum Vahl* extract as bio reductor and capping agent Published online 2020 Aug 7. doi: 10.1016/j.heliyon.2020.e04636.

[19] Synthesis and characterization of Al_2O_3 nanoparticles from Trachy spermum ammi Bibi E, J Agron Agri Sci 2023, 6: 050 DOI: 10.24966/AAS-8292/100050.

[20] Nduni MN, Osano AM, Chaka B (2021) Synthesis and characterization of aluminium oxide nanoparticles from waste aluminium foil and potential application in aluminium-ion cell. Cleaner Engineering and Technology 3: 100108.

[21] N.A.Bakr, A. M. Funde, V. S. Waman et al., "Determination of the optical parameters of a- Si: H thin films deposited by hot wire–chemical vapour deposition technique using transmission spectrum only," *Pramana: Journal of Physics*, vol. 76, no. 3, pp. 519–531, 2011.

[22] M. Srivastava, S. Chaubey, K. O. Animesh, Mater. Chem. Phy. **118,** 174 (2009).

[23] Ahmad RezaA bbasianand Mahdi Shafiee Afarani, One step solution combustion synthesis and characterization of $ZnFe_2O_4$ and $ZnFe_{1.6}O_4$ nanoparticles, *J.Appl.Phys. A.*125,(2019),1-12.

[24] Palusamy Suppuraj, Ganesamoorthy Thirunarayanan, Meenakshi sundaram Swaminathan and Inba sekaran Muthuvel, Facile Synthesis of Spinel Nanocrystalline $ZnFe_2O_4$: Enhanced Photo catalytic and Microbial Applications, *J.Mater Sci Technol,* 34, (2017)5-11.

[25] Hemmati,S. AhanyKamangar, A.Ahmeda, M.M.Zangeneh, A.Zangeneh, Application of copper nano particles containing natural compounds in the treatment of bacterial and fungal diseases, Appl.Organomet Chem.34(2020) 1-16, https://doi.org/10.1002/aoc.5465.

[26] A. Rameshwar Rao , V. Rajendar and K. Venkateswara Rao, "Structural and Optical Properties of ZnO Nano Particles Synthesised by Mixture of Fuel Approach in Solution Chemical Combustion," Advanced MaterialsResearch,629, pp.273-278,2013.

[27] K.TamizhSelvi, M.Rathnakumari, M.Priya and P.SureshKumar ,"Shape Transition Effect of Temperature on MgO Nanostructures and its Optical Properties, "International Journal of Scientific & Engineering Research, 5,pp. 60-64, 2014.

[28] Velumani S, Narayandass SaK, Mangalaraj D (1998) Structural characterization of hot wall Deposited selenide thin films. Semicond Sci Technol 13(1016–10).

[29] Ghosh A, Kumari N, Tewari S, Bhatta charjee A (2013) Structural and optical properties of pure and Al doped ZnO nanocrystals. Indian J Phys 87:1099–1104.https://doi.org/10.1007/s1264 013-0346-9.

[30] Nath, D.;Singh,F.;Das, R.X-ray diffraction analysis by Williamson- Hall, Halder-Wagner and size- strain plot methods of Cd Se nanoparticle-A comparative study. Mater. Chem. Phys. 2019,239,122021.

[31] Jacob, R.;Isac, J.X-ray diffraction line profile analysis of Ba 0. 6 Sr 0. 4 Fe xTi (1−x)O3-δ,(x=0.4).Int.J.Chem.Stud.2015,2, 12–21.

[32] A. I. Inamdar, Y. S. Kim, S. M. Pawar, J. H. Kim, H.Im and H. Kim, J. Power Sources (2011), 196, 239.